Solar Energy Materials & Solar Cells 119 (2013) 51–58

Contents lists available at ScienceDirect

Solar Energy Materials & Solar Cells

journal homepage: www.elsevier.com/locate/solmat

High-efficiency Cu(In,Ga)Se_2 cells and modules

Michael Powalla*, Philip Jackson, Wolfram Witte, Dimitrios Hariskos, Stefan Paetel, Carsten Tschamber, Wiltraud Wischmann

Zentrum für Sonnenenergie- und Wasserstoff-Forschung Baden-Württemberg (ZSW), Photovoltaics, Industriestr. 6, Stuttgart 70565, Germany

ARTICLE INFO

Available online 26 June 2013

Keywords:
Cu(In,Ga)Se_2
High-efficiency
Quality marker
Alternative buffer
Zn(O,S)

ABSTRACT

We report on the analytical description of high-efficiency Cu(In,Ga)Se_2-based solar cells produced with a static coevaporation process. We discuss classic quality markers such as grain morphology, composition, vertical compositional gradings, and grain orientation in these cells. We then describe the successful transfer of such results to industrially relevant inline processes in our module production line. Finally, we explicate one of the many optimisation routes for the further improvement of these Cu(In,Ga)Se_2-based solar cells: Zn(O,S) buffer layers.

1. Introduction

Solar cells based on Cu(In,Ga)Se_2 (CIGS) have reached conversion efficiencies above 20% [1,2]. This achievement demonstrates in principle that CIGS as an absorber material for solar modules can compete with multicrystalline silicon (mc-Si) based solar cells, where the record laboratory value of both technologies is in the same range [3]. So CIGS technology is the only concept which brings together a high-efficiency potential, large area coating, and monolithic integration. However, the commercial use of CIGS in the Gigawatt range, which means square kilometres of thin films, needs concepts that are capable to transfer the lab based results to cost effective industrial processes.

Whereas in the mc-Si technology the photovoltaic grade Si crystal has to be grown from the melt and the grain size must be in the centimetre range, photovoltaic grade CIGS can be grown as a thin-film with grains in the micrometre range comparable in size with the film thickness. For this thin-film growth, basically two methods are commonly used. On the one hand, thermal coevaporation of the elements Cu, In, Ga, and Se in vacuum at a high substrate temperature is used. With this process a very high film quality has been demonstrated [4]. On the other hand, reactive annealing of sputtered metal or alloy films is used in industry [5]. With the latter approach module efficiencies of 15.1% have been demonstrated so far [6]. Up to now all other process types such as reactive annealing of printed or electrodeposited precursors lead to significantly reduced material quality [7,8,9] and need more research in the laboratory before transferring them into industrial routes.

Due to low Si prices and other market effects, Si-based PV has been able to grow faster than thin-film technology in the past two years. Additionally, CIGS thin-film solar technology as applied in industry is still in an early development stage with still lingering potential for price reduction by scaling up fab size and standardising the production equipment. One way to speed up this development is to bring together equipment producers and industrial scale production. To overcome the challenge of the initial high investments to get a GW fab started, it is important that reasonable production costs can be reached in a smaller fab size first. Dimmler has reported that a 0.5 €/W_p production cost for a CIGS module production of 200 MW_p/a is feasible if laboratory results are transferred to the equipment design and processes quickly [4].

2. Experimental

2.1. Research cells

In order to facilitate the fast transfer of high-efficiency lab results to full scale production, we at the ZSW have divided our research in CIGS solar technology into three closely linked subsequent stages. The first is the investigation of a small area (0.50 cm^2) research cells. This stage is followed by the investigation of the same technology on a scaled-up prototype substrate size (30×30 cm^2) produced in industrially compatible inline machinery. The third development stage comprises the support of the implementation of this new technology into a fully scaled, high-speed, high-throughput industrial production line.

In the first stage of our research we focus on the exploitation of the maximum potential of thin-film solar technology by means of a

* Corresponding author: Michael Powalla. Tel.: +49 7117870263; fax: +49 7117870230.
E-mail addresses: michael.powalla@zsw-bw.de, michael.powalla@kit.edu (M. Powalla).

0927-0248/$ - see front matter © 2013 Elsevier B.V. All rights reserved.
http://dx.doi.org/10.1016/j.solmat.2013.05.002

small-area high-efficiency production line. The heart of this line is a high-vacuum cluster deposition system that allows the static coevaporation of the CIGS absorber's constituent elements and the sputter deposition of i-ZnO and ZnO:Al as window materials. The static deposition in these processes enables us to be very flexible in the variation of the process parameter. This flexibility allows us, quite in contrast to larger inline prototype processing equipment, to try new process paths very easily with no or very little adaption of the processing hardware.

In addition, the cluster vacuum system makes it possible to employ a full insitu deposition of a CIGS solar cell starting from the Mo layer up to the ZnO window layer deposition. However, up to now buffer layers deposited by exsitu chemical bath deposition (CBD) still yield the best device results. We therefore also break the vacuum after the CIGS growth to deposit the buffer in a wet chemical process.

As a substrate we use both standard soda-lime glass (3 mm) and for practical purposes also use some thinner (2 mm) alkali-aluminosilicate glass. The vacuum deposited thin-film stack consists of sputtered molybdenum (500–900 nm) functioning as a back contact, CIGS (2.5–3.0 μm) as the absorber material, chemical bath deposited CdS as buffer layer (40–50 nm), sputtered undoped ZnO (50–100 nm), sputtered Al-doped ZnO (150–200 nm) as conductive window material, and a nickel/aluminium grid. For high-efficiency cells we additionally put an anti-reflective coating (ARC) on top of that (MgF_2/105 nm). Finally, the cell size is defined by mechanical scribing. The cell area is 0.50 cm^2 with very little variation.

One of our major goals in small area CIGS research is to increase the reproducibility of high efficiencies beyond 20% in order to better understand and control the quality determining factors of CIGS cell production. For this purpose we emphasise on the reproducibility and control of processing conditions. Once a larger set of high-efficiency cells is available, the results of analytical investigations of these cells yield higher statistical significance and higher industrial relevance. This enlarged scientific basis makes the transfer of this still rather new solar technology much easier and faster.

2.2. Modules

As the transfer of new renewable energy technologies into industrial production is the goal of the ZSW, we consequently, in a second stage of research, operate processing equipment that is very close to that of an industrial environment. For this purpose we have set up a module line that employs inline deposition systems for all production steps. The prototype substrate size is 10×10 cm^2 and 30×30 cm^2. In order to be able to transfer the high-efficiency CIGS process from the static deposition, we have set up the inline CIGS deposition system as a multi-stage process that allows for an independent rate and temperature control in more than one deposition step [10]. Near industrial conditions are realised also by the establishment of a production corridor in our R&D line that gets the modules from CIGS deposition to current–voltage measurement within less than 36 h. The cell stack is similar to the small area cells except for a thicker aluminium doped ZnO in the case of the modules (900 nm) and the replacement of the metallic grid by the monolithic module integration.

2.3. Exemplary optimisation route—alternative buffers

There are many elements, layers, process steps, and parameters that need to be optimised in order to produce high efficiencies—both in small area cells and large area modules. In this paper we describe one of these elements as an exemplary optimisation route: Zn(O,S) as an alternative buffer. Typically, our standard CIGS-based solar cells contain a 50 nm chemical bath deposited CdS buffer layer between the light absorbing CIGS layer and the transparent conducting ZnO front electrode. The growth of the CdS layer on CIGS takes place in an ammonia, cadmium sulphate, and thiourea containing solution at temperatures in the range of 60–65 °C [11].

As an alternative to the CdS, a CBD Zn(O,S) buffer has been established in our lab, which can be deposited by two different approaches [12]:

(a) … by a relatively slow procedure using a $ZnSO_4$/NH_4OH/thiourea solution at temperatures of 80 °C, which is, from a chemical point of view, quite similar to the standard CdS process.
(b) … by a much faster deposition process using $ZnSO_4$ as the metal source, a mixture of ammonia and sodium nitrilotriacetate (Na_3NTA) as the complexing agent, and thioacetamide (TAA) as the sulphide source.

Devices with a standard CdS buffer are completed with an i-ZnO/ZnO:Al bilayer, while in cells with a CBD Zn(O,S) buffer a high resistivity (Zn,Mg)O layer is used as substitute for the undoped i-ZnO [13].

3. Characterisation methods

For small area cells current–voltage (j–V) analysis was performed under a simulated AM 1.5 G spectrum at 25 °C with a four-point measurement setup. Note, that all results represent in-house measurements with ARC except where explicitly stated. CIGS composition was determined with an X-ray fluorescence spectroscopy (XRF) instrument from EDAX (Eagle XXL).The investigation of grain orientation of the CIGS absorber was performed using a X-ray diffractometer (XRD) from PANalytical Empyrian with Cu K_α radiation in Bragg–Brentano geometry. For compositional depth-profiling of the CIGS absorber, glow discharge optical emission spectroscopy (GDOES) was employed (GD-PROFILER 2, Horiba Jobin Yvon) with an Ar^+-ion beam resulting in a sputter crater with a diameter of 4 mm. Finally, we have studied the film morphology with a scanning electron microscope (SEM) XL30 SFEG Sirion from FEI. It must be noted that all analytical investigations on high-efficiency cells have been performed at exactly the same position where the electrical j–V data had been taken from.

4. Results

4.1. Research cells

After having passed the 20% efficiency barrier with small area CIGS solar cells, it has been a major goal for us to better understand and describe the processes that have led us to this performance level as well as the devices themselves. The better we understand these processes, the higher is the reproducibility, and the better we understand the devices, the easier it is to monitor device quality in an altered production setting as in industrial application. Eventually, this will improve our capability to efficiently transfer high-efficiency lab results to industrial production. This part of the contribution now aims at the analytical description of the high-efficiency devices.

In Table 1 we list a small selection of 20% cells (samples 1–15) with their basic current–voltage parameters and the overall composition ratios [Cu]/([Ga]+[In]) (CGI) and [Ga]/([Ga]+[In]) (GGI) as derived from XRF. Apart from the 15 cells from the small area production line, we have, for the sake of comparison, added three small area cells that were produced in our 30×30 cm^2

Table 1
High-efficiency CIGS solar cells from a static (and in-line) deposition process with conversion efficiency η, open-circuit voltage V_{OC}, short-circuit current density j_{SC} and fill factor *FF* from *j–V* measurements (in-house). [Cu]/([Ga]+[In]) (CGI) and [Ga]/([Ga]+[In]) (GGI) ratios are derived from XRF and $I_{220/204}$: I_{112} from XRD (discussion see further below) measurements.

Sample no.	CIGS process	η (%)	V_{OC} (mV)	j_{SC} (mA/cm^2)	*FF* (%)	CGI	GGI	XRD $I_{220/204}$: I_{112}
1	Static	20.4	741	35.4	77.8	0.92	0.33	1.7
2	Static	20.3	728	35.7	77.9	0.90	0.31	–
3	Static	20.3	724	36.2	77.2	0.87	0.33	0.9
4[a]	Static	20.3	740	35.4	77.5	0.88	0.34	0.9
5	Static	20.3	735	35.5	78.0	0.93	0.33	1.5
6	Static	20.3	741	35.5	77.5	0.90	0.33	1.8
7	Static	20.2	739	35.3	77.3	0.89	0.33	1.9
8	Static	20.2	726	35.5	78.4	0.93	0.32	4.6
9	Static	20.2	731	35.3	78.1	0.89	0.32	4.0
10	Static	20.1	713	36.4	77.3	0.92	0.32	2.8
11	Static	20.1	711	36.1	78.5	0.89	0.32	1.5
12	Static	20.1	726	35.6	77.6	0.86	0.32	3.4
13	Static	20.1	738	35.1	77.6	0.89	0.34	4.1
14	Static	20.0	740	34.4	78.7	0.89	0.36	3.5
15	Static	20.0[b]	717	36.3[b]	76.9	0.90	0.32	0.3
16	Inline	19.2[b]	689	34.5[b]	80.6	0.83	0.27	0.4
17	Inline	19.2[b]	692	34.8[b]	79.7	0.85	0.29	0.4
18	Inline	18.7[b]	688	34.5[b]	78.6	0.83	0.27	0.4
19	Static	18.2[b]	717	34.3[b]	74.0	0.89	0.36	37.0
20	Static	19.2[b]	693	35.6[b]	77.9	0.89	0.30	15.0

[a] Certified by Fraunhofer ISE (June 2010).
[b] ARC-equivalent values (i.e. +1% in efficiency added to the non-ARC value; j_{sc} adapted appropriately).

substrate size formatted inline module production line. As we have described elsewhere [2], on a 20% efficiency level the overall composition can still be varied quite a bit (0.30≤GGI≤0.34 and 0.80≤CGI≤0.92). The current results, however, push the efficiency range for which these values are valid further up to 20.0–20.4% (in-house measurements) and additionally expand the overall composition range even further to 0.30≤GGI≤0.36 and 0.80≤CGI≤0.93.

However, the variability that we see in CIGS cells with an efficiency level of 20.0–20.4% is not confined to the overall composition but extends also to other traditional quality markers as the morphology of the CIGS absorber.

This fact can be seen in Fig. 1 where we do not see a consistent pattern of only large grains for high-efficiency cells. Although we observe large grains with a diameter of approximately 2 μm in all three examples, we always see smaller grains right beside these as well. Fig. 1(a) shows only a few smaller grains with a diameter of approximately 0.5–1.0 μm, in Fig. 1(b); however, nearly all of the left half of the cross-section is filled with grains of that smaller size, and in Fig. 1(c) we even find a continuous bottom layer of 0.5 μm thickness that consists of grains with a diameter of only 0.2–0.5 μm. In addition, we find large voids between this small grained bottom layer and the top layer of large grains. The efficiencies of these SEM analysed solar cell samples, however, are practically the same.

Depth profiling of these high-efficiency CIGS absorbers performed with GDOES at first reveals an up-to-date double-graded composition (Fig. 2(a)): high GGI at the back contact, low GGI minimum near the front part, rising GGI towards the surface, and In-rich and Cu-depleted surface composition. The efficiency of 20.4% seems to match the expectations of a perfectly graded absorber. However, Fig. 2(b) shows deviations from this seeming optimum. In fact, the double-grading in its classical shape is present, yet, the surface composition deviates notably from Fig. 2(a) with hardly any decrease in GGI and Cu content at the surface. In addition, the $MoSe_2$ peak (correlates with the Se/CIGS × 100 signal) at the back contact is smaller compared to sample no. 1. The solar cell conversion efficiencies of samples 1 (20.4%) and 5 (20.3%), however, are the same. Almost pathological with regard to the

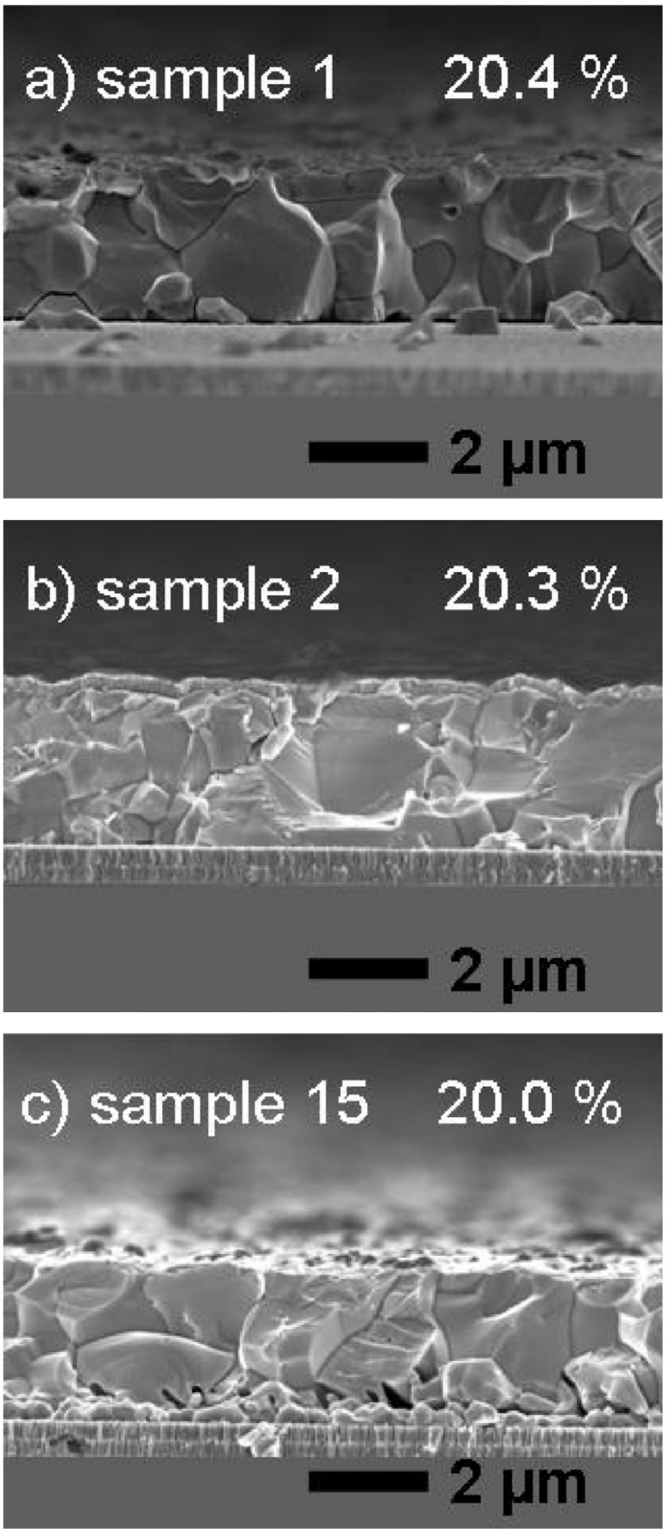

Fig. 1. SEM pictures of cross-section for (a) sample 1 (η=20.4%), (b) sample 2 (η=20.3%), and (c) sample 15 (η=20.0%). The crystal morphology varies notably despite the similar efficiency level.

goal of high-efficiency is the GGI grading profile for sample no. 15 in Fig. 2(c): the GGI is not high at all at the back contact (i.e. hardly any back surface field). In addition, the GGI increases towards the front, but is higher at the front than at the back. Nevertheless, the efficiency of 20.0% is still very well on the same level as the ones of samples 1 and 5. Thus, once more we see a significant variation in a quality

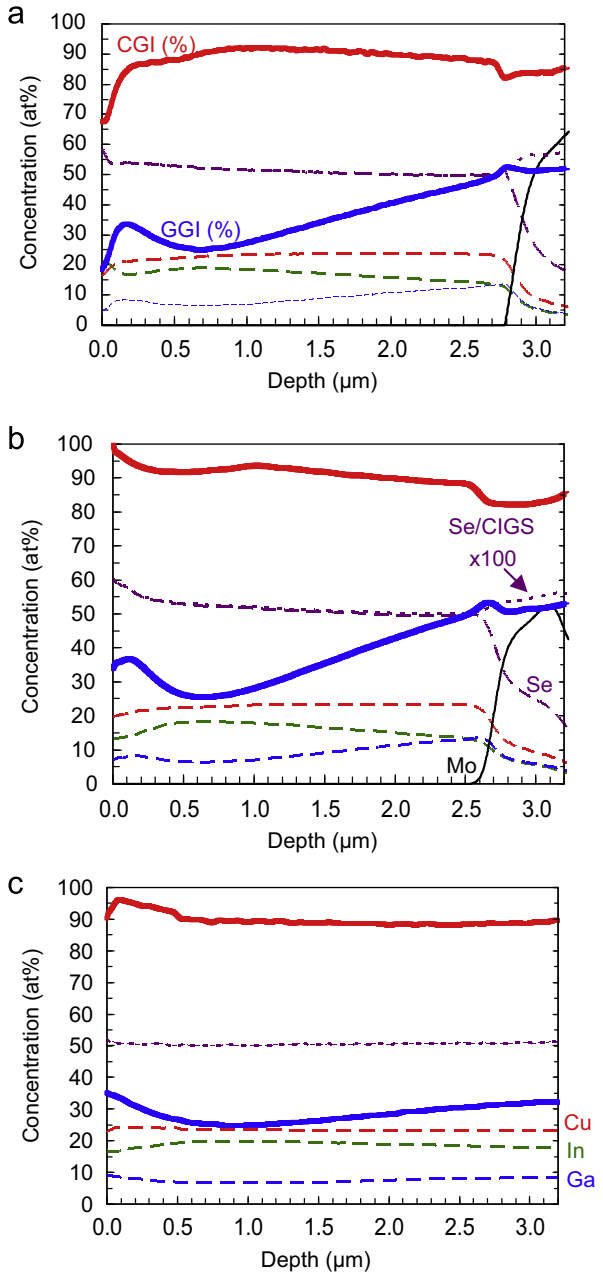

Fig. 2. GDOES depth profile of CIGS absorbers for (a) sample no. 1 (η=20.4%), (b) sample no. 5 (η=20.3%) and (c) sample no. 15 (η=20.0%).

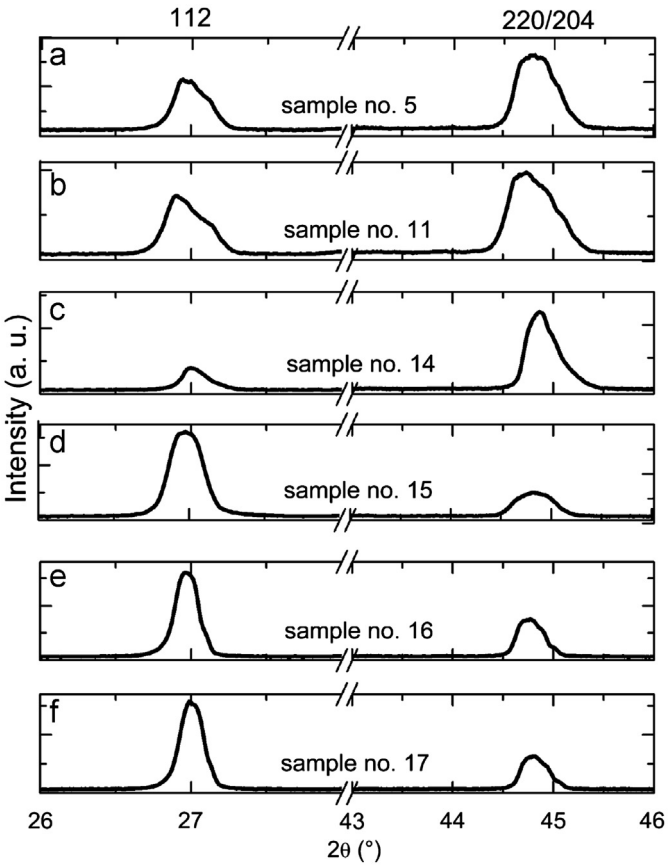

Fig. 3. XRD patterns of CIGS deposited by the static (a–d) and in-line (e and f) process on Mo-coated glass substrates. CIGS layers are from the same selection of cells as listed in Table 1.

marker (compositional grading) that is frequently discussed in literature and often associated with high-efficiency CIGS solar cells [14–18].

Apart from overall composition, grain size, and various types of vertical gradings, we have also investigated the absorber in more detail by looking at the orientation of the grains. Fig. 3 depicts XRD patterns of a selection of the high-efficiency cells as listed in Table 1. They have been recorded after the removal of buffer and window layers by a diluted HCl etch. It is obvious from the intensity ratios of the 220/204 and 112 reflexes ($I_{220/204}$: I_{112}) (see also Table 1), that we can achieve high-efficiency cells with the static deposition process exhibiting different bulk orientations. Sample nos. 5 and 11 (Fig. 3(a and b)), for example, exhibit a ⟨110⟩/⟨201⟩ orientation which is typical for CIGS grown by multiple deposition steps involving a Cu-rich growth phase [19,20]. Sample no. 14 (Fig. 3(c)) shows an even stronger ⟨110⟩/⟨201⟩ orientation. The CIGS grains of sample no. 15 (Fig. 3(d)), however, also deposited by the static process, are oriented more randomly ($I_{220/204}$: I_{112}≈0.3) with a slight tendency to ⟨221⟩ (randomly oriented CIGS exhibits a ratio of $I_{220/204}$: I_{112}=0.4). The latter result is very similar to our CIGS from the inline deposition process (sample nos. 16 and 17 in Fig. 3(e and f)). Furthermore, it can be noted that these two inline samples and sample no. 15 from the static process exhibit a symmetric 112 reflex whereas the remaining absorbers from the static process showed a prominent splitting. The splitting of this reflex can be interpreted as a result of strong vertical changes in the GGI ratio as reported by several groups [21,22,18].

This conclusion can be verified for our results by referring back to the GDOES depth profiles in Fig. 2. Sample nos. 5 and 14 (not shown) show a strong GGI gradient. Consequently, they exhibit the splitting of the 112 reflex. On the other hand, sample no. 15 has almost no GGI gradient and thus a symmetric 112 reflex.

The fact that we have obtained CIGS solar cells with conversion efficiencies above 20% with different degrees of orientation of the CIGS grains is further illustrated in Fig. 4. For these high-efficiency cells (samples 1–15) we find a considerable variation in the characteristic XRD reflex intensity ratio: $0.3 \le I_{220/204} : I_{112} \le 4.6$. This finding is in contrast to reports from Chaisitsak et al. [23] who have observed a drop in efficiency on both sides within the range of peak ratios mentioned above.

If we additionally allow more extreme XRD bulk values to be added to the data set of Fig. 4, it seems as if the high efficiencies cannot be kept up on both sides of the spectrum (see Fig. 5). However, the statistical basis for a clear trend is still too thin for drawing firm conclusions. And when evaluating this data set, it further must be taken into account that cells produced in the inline production line (circular symbols) have received window layers that are not as well optimised as in the case of the small

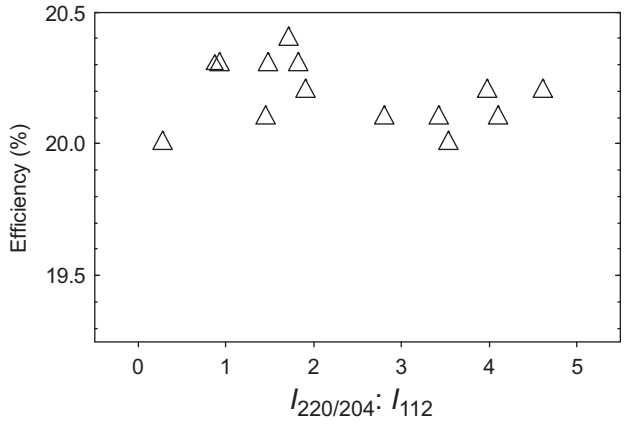

Fig. 4. CIGS solar cells with conversion efficiencies $\eta \geq 20\%$ grown with the static deposition process (sample nos. 1–15). The absorbers exhibit different bulk orientations as derived from XRD despite the same efficiency level of the corresponding solar cells.

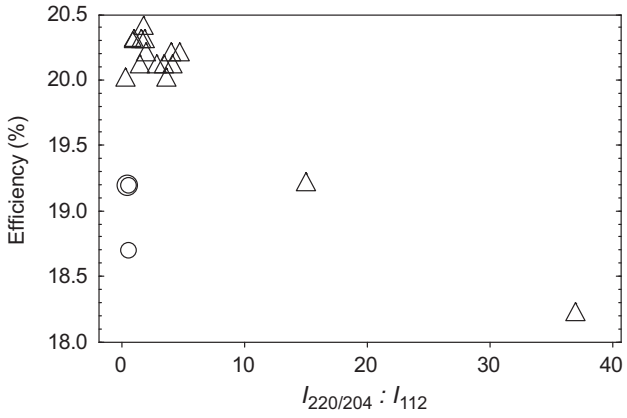

Fig. 5. Preliminary experimental relationship between cell efficiency and CIGS grain orientation (XRD). Samples (nos. 1 to 20, see Table 1) are produced in different deposition processes: static (triangles) and inline (circles).

area production line. Nevertheless, the data can be taken as a start for further investigations.

On the whole we can state from our small area cell research that classic quality markers as CIGS absorber grain size, void formation, and composition often fail to distinctly describe high quality in CIGS solar cells. But, in addition, even more distinguished approaches as detailed vertical compositional profiles and grain orientation do not necessarily reduce the ambiguity. However, it is important to note that we do not claim the total irrelevance of these parameters. We only state the fact that in all of these quality markers we still see a considerable variability on a very high 20.0–20.4% efficiency level, which for us still indicates a lack of saturation in the development of maximum CIGS efficiencies, which is a promising outlook for the ongoing transfer of this technology to large scale production.

4.2. Modules

In order to further improve CIGS solar module efficiencies, we have performed various optimisation cycles in the different process steps. Three patterning steps (P1, P2, and P3) are necessary to realise the monolithically integrated module connection. The first of these (P1) has to go through the CIGS sequence. The subsequent patterning lines have to be set as close to the first line as possible. The width of the patterning lines is 60 μm and our original distance between the lines used to be 150 μm (Fig. 6(a)). The improved procedure reduced the distance between P1 and P2 to 100 μm and between P2 and P3 down to 75 μm (Fig. 6(b)). This reduction of the dead area between P1 and P3 gives rise to a relative increase of the active area of 2.9% in each module cell with a direct considerable impact on j_{sc} and the efficiency of the modules.

A further characteristic feature of the CIGS process that we employ in our inline machine is the multistage approach [10]. This approach comprises of a controlled route across the stoichiometric point of the CIGS crystal into the Cu-rich regime and back to slightly Cu-poor. However, the “if”, the “how”, and “when” of this route is crucial for high module efficiencies. For this reason it is essential to be able to control this parameter. In a static deposition process, classic end-point detection methods can be employed. In an inline deposition process, however, this is much harder to accomplish. One possible method to realise an end-point detection in an inline process with a moving substrate is laser-light scattering (LLS) which has originally been developed at Helmholtz-Zentrum Berlin in a static deposition and has first been implemented in an inline system at ZSW in a joint project (LARCIS project: FP-6-019757 funded by the European Commission) [24]. In Fig. 7(a and b)) the configuration of the LLS in our inline system and the corresponding signals Fig. 7(c) of modules in a CIGS run with slowly increasing Cu rate (i.e. Cu maximum height) are depicted. In Fig. 7(c) the Cu content of the finished device is noted, which correlates with the Cu maximum height beyond 25 at% in the deposition stage investigated here by LLS. An increase of the height of the Cu maximum in the Cu-rich regime during a CIGS run in Fig. 7(c) obviously shifts back to the maximum reflection signal intensity in the respective part of the deposition chamber (from right to left). The change in reflectivity is due to the change in surface roughness when going from Cu-poor to Cu-rich composition in CIGS multistage processing. With LLS we have a visible signal and a precise tool for monitoring the end-point procedure in an inline deposition.

In the deposition of the aluminium doped ZnO front contact the following adjustments to the former standard procedure has lead to a noticeable performance boost in the finished devices.

The exact temperature characteristic over time in the process is crucial for the highest quality in the window layer and was adjusted appropriately. This includes the precise control of the carrier temperature before the deposition and the reduction of the critical temperature in the load-lock and deposition chambers.

In order to accelerate the overall optimisation process, we have for practical purposes opted for the 10×10 cm² format instead of the 30×30 cm^2. The smaller substrate size still incorporates all the features of a full-size module but enables us to conduct the experiments with a more reliable statistical validation basis in runs with limited capacity. Fig. 8 depicts our best result in the 10×10 cm^2 format with 16.8% (w/ARC; certified by Fraunhofer ISE).

4.3. Exemplary optimisation route—alternative buffers

CIGS cells with the Zn(O,S)/(Zn,Mg)O buffer structure often reach their maximum conversion efficiency after post-annealing in air at 200 °C for up to 30 min followed by a light soaking procedure under one sun for several minutes or hours at room temperature or at elevated temperatures up to 80 °C [25,26]. However, from a technological point of view this post-annealing procedure is an issue for a production line because it requires an additional step and additional equipment.

Based on the CBD Zn(O,S) recipe via thiourea as organosulfide the buffer layer deposition time was varied from 0 to 40 min. This yielded a Zn(O,S) thickness variation in the range of 0–40 nm as determined by SEM. The solar cell parameters of the as-grown Zn

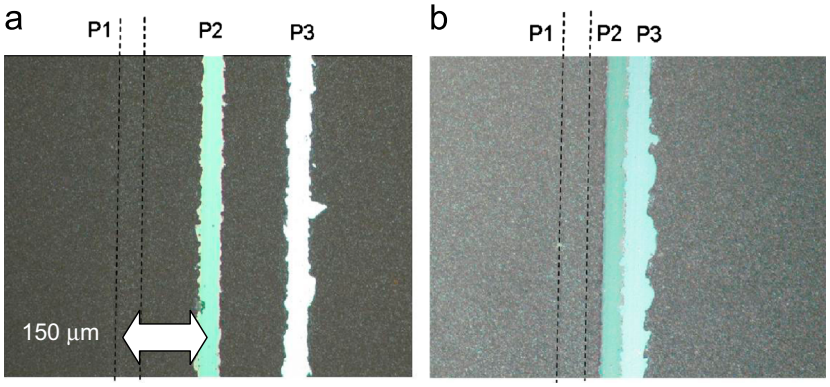

Fig. 6. Light microscopic images of a monolithic cell connection in a CIGS module depicting P1, P2 and P3 in (a) standard configuration (150 µm spacing) and (b) with reduced spacing.

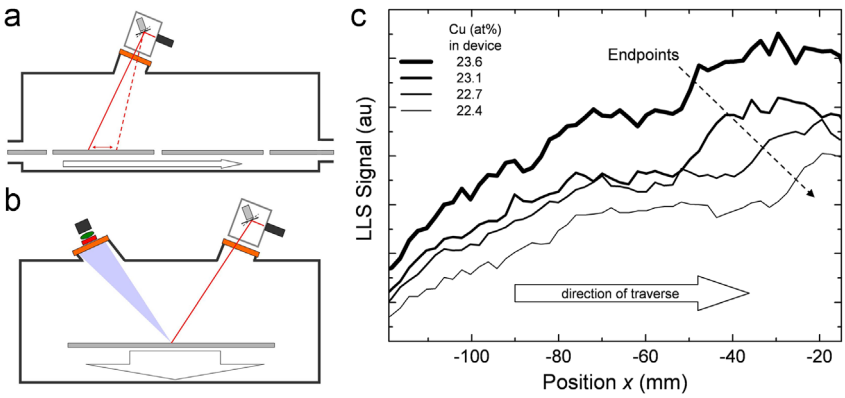

Fig. 7. Schematic diagram of a laser-light scattering system LLS for end-point detection in an inline deposition system (a) side view (laser beam is scanned continually back and forth along the direction of traverse), (b) cross-sectional view (laser beam port and detector port) and (c) the reflected laser light intensity increases distinctly at the point where the CIGS absorber crosses into the Cu-rich regime. This point shifts in its position along the direction of traverse when the degree of Cu-excess varies during a CIGS run.

(O,S)-buffered cells as well as the influence of post-annealing in air are depicted in Fig. 9 in comparison to the reference cells with the traditional CdS/i-ZnO buffer system.

The CIGS solar cells with the Zn(O,S)/(Zn,Mg)O buffer in this experiment (inline process) reach conversion efficiencies in the range of 12–16%. The cells without Zn(O,S), i.e. with (Zn,Mg)O directly sputtered on the CIGS layer, exhibit efficiencies around 9%. With increasing Zn(O,S) buffer thickness the efficiency increases, mainly due to an enhancement in V_{OC}. This trend was also reported by Nakada et al. for CIGS cells with CBD Zn(O,S) buffers with thicknesses between 80 and 120 nm [27]. The reason for this effect could not be only a thickness effect of Zn(O,S), improving thereby also the coverage of the differently oriented CIGS grains [28], but also an effect of increased zinc diffusion from the chemical bath or the deposited Zn(O,S) into the CIGS layer with the progress of deposition time at the relatively high bath temperature of 80 °C [29,26]. However, this topic is a subject of future investigations.

Post-annealing in air at 200 °C for 30 min leads to an efficiency improvement for all cells with thinner Zn(O,S) buffer (t_{dep} = 10 min and t_{dep} = 18 min), which is influenced by an increase in V_{OC} and j_{SC}. Cells with thicker Zn(O,S) grown at longer deposition times (t_{dep} = 28 min and 40 min) show no efficiency increase after the annealing step similar to the behaviour of the reference cells with the CdS buffer. The fill factor *FF* for all Zn(O,S) thicknesses is not significantly affected by heating the cells in air. The behaviour of cells without a Zn(O,S) buffer is an exception. Here, the post-annealing has a detrimental effect on all solar cell parameters except the j_{SC}.

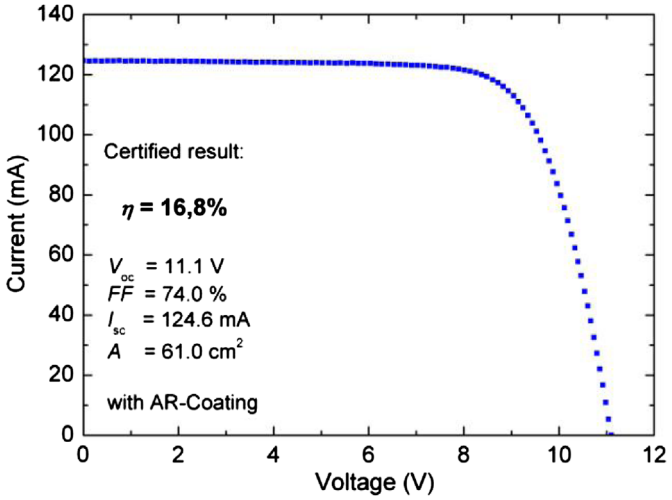

Fig. 8. Current–voltage curve of the best 10 × 10 cm² module: 16.8% efficiency (w/ARC; aperture area efficiency; certified by Fraunhofer ISE).

5. Conclusion

We have shown that the employment of all development steps in one research institute provides a good ground for a fast and efficient transfer of the CIGS solar technology. In particular we could prove that despite a very high level in conversion

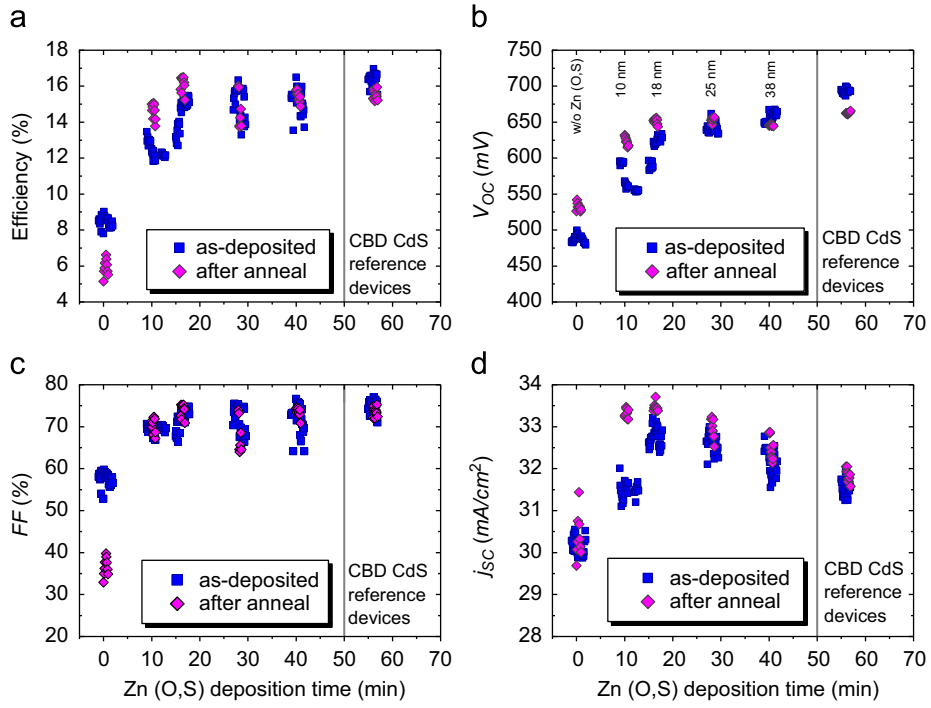

Fig. 9. Device parameters of small-area CIGS (inline process)/Zn(O,S)/(Zn,Mg)O/ZnO:Al cells dependent on the deposition time and thickness compared to reference cells with a standard CBD CdS/i-ZnO buffer system. The influence of post-annealing at 200 °C for 30°/min in air (rhombuses) is compared to the as-deposited state (squares). (a) efficiency, (b) open-circuit voltage V_{OC}, (c) fill factor *FF* and (d) short-circuit current density j_{SC}. Zn(O,S) thicknesses indicated in (b) are determined from SEM cross-sections.

efficiencies in small area cells above 20% we can still observe considerable variability in some of the classic quality markers for such devices (i.e. $0.30 \le GGI \le 0.36$ and $0.80 \le CGI \le 0.93$; variable grain sizes; $0.3 \le I_{220/204} : I_{112} \le 4.6$). We interpret this phenomenon of wide process windows on a high-efficiency level as an indication for very good suitability of the CIGS technology for high volume production. And we further conclude that the efficiency development for CIGS technology is still in a non-saturated stage. On the basis of these results we have been able to successfully transfer the high-efficiency lab results to an industrially relevant inline module production line with module efficiencies reaching up to 16.8%. As a consequence of such continual research and the cooperation of the ZSW with the MANZ AG, the MANZ AG recently was able to produce one of the highest efficiencies for an industrially produced large area thin-film solar module ever. This top efficiency value of 14.6% (15.9% aperture area/104.8 W) [30] shows once more that the new CIGS solar technology is the most promising thin-film candidate to offer a competitive alternative for the current silicon technologies. It has a high potential for both cost reduction and high efficiencies. Thus it appears feasible to transfer the very high CIGS small area solar cell efficiencies of this new thin-film solar technology from the lab to industry successfully.

Acknowledgements

The authors gratefully acknowledge the support of Dieter Richter (small area cell production), Wolfgang Dittus, Andreas Nowitzki, Frank Nauerz, Christine Boehmerle, and Daniela Müller (module production), Tania Wonhaas (SEM), Wolfram Hempel (GDOES), and the funding by the state of Baden-Württemberg (ministry of economics) and by the Bundesministerium für Umwelt, Naturschutz und Reaktorsicherheit (BMU) under Contract- no. 0329585G.

References

[1] EMPA Press Release (January 2013): ⟨http://www.empa.ch/plugin/template/empa/*/79143⟩.
[2] P. Jackson, D. Hariskos, E. Lotter, S. Paetel, R. Wuerz, R. Menner, W. Wischmann, M. Powalla, New world record efficiency for Cu(In,Ga)Se_2 thin-film solar cells beyond 20%, Progress Photovoltaics: Research Applications 19 (2013) 894–897.
[3] M.A. Green, K. Emery, Y. Hishikawa, W. Warta, E.D. Dunlop, Solar cell efficiency tables (version 41), Progress Photovoltaics: Research Applications 21 (2011) 1–11.
[4] B. Dimmler, CIGS and CdTe based thin film PV modules, an industrial revolution, Proceedings of the Photovoltaic Specialists Conference (PVSC), Austin, Texas, USA002494–002499.
[5] K. Kushiya, $CuInSe_2$-based thin-film photovoltaic technology in the Gigawatt production era, Japnaese Journal of Applied Physics 51 (2012) 10NC01-1–10NC01-5.
[6] TSCM Press Release (January 2013): ⟨http://www.tsmc-solar.com/Assets/downloads/en-GB/TSMC_Solar_Press_Release_EN_Jan_31_2013.pdf⟩.
[7] I. Klugius, R. Miller, A. Quintilla, T.M. Friedlmeier, D. Blázquez-Sánchez, E. Ahlswede, M. Powalla, Rapid thermal processing for printed Cu(In,Ga)$(S,Se)_2$ solar cells: comparison of precursor materials, Thin Solid Films 535 (2013), 107–111.
[8] A. Cho, S. Ahn, J.H. Yun, J. Gwak, S.K. Ahn, K. Shin, H. Song, K.H. Yoon, Non-vacuum processed $CuInSe_2$ thin films fabricated with a hybrid ink, Solar Energy Materials and Solar Cells 109 (2013) 17–25.
[9] T.K. Todorov, O. Gunawan, T. Gokmen, D.B. Mitzi, Solution-processed Cu(In,Ga)$(S,Se)_2$ absorber yielding a 15.2% efficient solar cell, Progress Photovoltaics: Research Applications 21 (2013) 82–87.
[10] G. Voorwinden, R. Kniese, P. Jackson, M. Powalla, In-line Cu(In, Ga)Se_2 Co-evaporation process on 30cm × 30cm substrates with multiple deposition stages, in: Proceedings of the 22nd EU PVSEC, Milan, Italy, September 3–7, 2007, pp. 2115–2118.
[11] J. Kessler, K.O. Velthaus, M. Ruckh, R. Laichinger, H.W. Schock, D. Lincot, R. Ortega, J. Vedel, Chemical bath depostion of CdS on $CuInSe_2$, etching effects and growth kinetics, in: Proceedings of the 6th International Photovoltaic Science and Engeneering Conference (PVSEC-6), New Delhi, India, February 10–14, 1992, pp. 1005–1010.
[12] D. Hariskos, R. Menner, P. Jackson, S. Paetel, W. Witte, W. Wischmann, M. Powalla, L. Bürkert, T. Kolb, M. Oertel, B. Dimmler, B. Fuchs, New reaction kinetics for a high-rate chemical bath deposition of the Zn(S,O) buffer layer for Cu(In,Ga)Se_2-based solar cells, Progress Photovoltaics: Research Applications 20 (2012) 534–542.
[13] D. Hariskos, B. Fuchs, R. Menner, N. Naghavi, C. Hubert, D. Lincot, M. Powalla, The Zn(S,O,OH)/ZnMgO buffer in thin-film Cu(In,Ga)$(Se,S)_2$-based solar cells Part II: magnetron sputtering of the ZnMgO buffer layer for in-line

co-evaporated Cu(In,Ga)Se_2 solar cells, Progress Photovoltaics: Research Applications 17 (2009) 479–488.
[14] A.M. Gabor, J.R. Tuttle, D.S. Albin, M.A. Contreras, R. Noufi, High-efficiency $CuIn_xGa_{1-x}Se_2$ solar cells made from $(In_x,Ga_{1-x})_2Se_3$ precursor films, Applied Physical Letters 65 (1994) 198–200.
[15] T. Dullweber, G. Hanna, W. Shams-Kolahi, A. Schwartzlander, M.A. Contreras, R. Noufi, H.W. Schock, Study of the effect of gallium grading in Cu(In,Ga)Se_2, Thin Solid Films 361–362 (2000) 478–481.
[16] M. Gloeckler, J.R. Sites, Band-gap grading in Cu(In,Ga)Se_2 solar cells, Journal of Physics and Chemistry of Solids 66 (2005) 1891–1894.
[17] S. Schleussner, U. Zimmermann, T. Wätjen, K. Leifer, M. Edoff, Effect of gallium grading in Cu(In,Ga)Se_2 solar-cell absorbers produced by multi-stage coevaporation, Solar Energy Materials and Solar Cells 95 (2011) 721–726.
[18] A. Chirila, S. Buecheler, F. Pianezzi, P. Bloesch, C. Gretener, A.R. Uhl, C. Fella, L. Kranz, J. Perrenoud, S. Seyrling, R. Verma, S. Nishiwaki, Y.E. Romanyuk, G. Bilger, A.N. Tiwari, Highly efficient Cu(In,Ga)Se_2 solar cells grown on flexible polymer films, Nature Materials 10 (2011) 857–861.
[19] M.A. Contreras, B. Egaas, K. Ramanathan, J. Hiltner, A. Swartzlander, F. Hasoon, R. Noufi, Progress toward 20% efficiency in Cu(In,Ga)Se_2 polycrystalline thin-film solar cells, Progress Photovoltaics: Research Applications 7 (1999) 311–316.
[20] D. Rudmann, G. Bilger, M. Kaelin, F.J. Haug, H. Zogg, A.N. Tiwari, Effects of NaF coevaporation on structural properties of Cu(In,Ga)Se_2 thin films, Thin Solid Films 431–432 (2003) 37–40.
[21] M.A. Contreras, J. Tuttle, A. Gabor, A. Tennant, K. Ramanathan, S. Asher, A. Franz, J. Keane, L. Wang, J. Scofield, and R. Noufi, High efficiency Cu(In,Ga)Se_2-based solar cells: processing of novel absorber structures, in: Proceedings of the First WCPEC, Hawaii, December 5–9, 1994.
[22] O. Lundberg, J. Lu, A. Rockett, M. Edoff, L. Stolt, Diffusion of indium and gallium in Cu(In,Ga)Se_2 thin film solar cells, Journal of Physics and Chemistry of Solids 64 (2003) 1499–1504.
[23] S. Chaisitsak, A. Yamada, M. Konagai, Preferred orientation control of $Cu(In_{1-x}Ga_x)Se_2$ (x≈0.28) thin films and its influence on solar cell characteristics, Japanese Journal of Applied Physics 41 (2002) 507–513.
[24] R. Scheer, A. Pérez-Rodríguez, W.K. Metzger, Advanced diagnostic and control methods of processes and layers in CIGS solar cells and modules, Progress Photovoltaics: Research Applications 18 (2010) 467–480.
[25] D. Hariskos, B. Fuchs, R. Menner, M. Powalla, N. Naghavi, D. Lincot, The ZnS/ZnMgO buffer combination in CIGS-based solar cells, in: Proceedings of the 22nd European Photovoltaic Solar Energy Conference, Milan, Italy, September 3–7, 2007, pp. 1907–1910.
[26] W. Witte, D. Hariskos, A. Eicke, R. Menner, O. Kiowski, M. Powalla, Impact of annealing on Cu(In,Ga)Se_2 solar cells with Zn(O,S)/(Zn,Mg)O buffers, *Thin Solid Films* 535, 2013, 180-183.
[27] T. Nakada, K. Furumi, A. Kunioka, High-efficiency cadmium-free Cu(In,Ga)Se_2 thin-film solar cells with chemically deposited ZnS buffer layers, IEEE Transactions on Electron Devices 46 (1999) 2093–2097.
[28] W. Witte, D. Abou-Ras, D. Hariskos, Chemical bath deposition of Zn(O,S) and CdS buffers: influence of Cu(In,Ga)Se_2 grain orientation, Applied Physics Letters 102 (2013) 051607–1–051607–4.
[29] J. Bastek, N.A. Stolwijk, R. Wuerz, A. Eicke, J. Albert, S. Sadewasser, Zinc diffusion in polycrystalline Cu(In,Ga)Se_2 and single-crystal $CuInSe_2$ layers, Applied Physics Letters 101 (2012) 074105-1–074105-3.
[30] MANZ press release (October 2012): ⟨http://www.manz.com/media/news/archive/2012⟩.